Intra- and intercellular immune responses across diverse *in vitro* stimuli and inflammatory disease

Authors:

Oliver Wood[1*], Adam T. Braithwaite[1*], Josephine Fisher[1], Li Li[2], Lynne Murray[1], Christopher Paluch[1], Matthew A. Jackson-Wood[1]

Institutional Affiliation:

[1] Gilead Sciences, 9400 Oxford Business Park, Garsington, Oxford OX4 2HN

[2] Gilead Sciences, 333 Lakeside Dr, Foster City, CA 94404, USA

* Authors contributed equally

Abstract

In vitro stimulation of healthy human immune cells is commonly used to reproduce the immune states observed in disease, both to understand pathology and to test therapeutic approaches. However, experiments typically focus on individual cell types and stimuli and a comprehensive cellular comparison of common immunomodulators and their relevance to disease is lacking. To this end, we performed integrated single-cell transcriptomic profiling of human peripheral blood mononuclear cells treated with 11 different common *in vitro* stimuli, totalling over 150,000 cells from 21 immune cell subtypes. Comparative analysis of the immunomodulations revealed their shared and unique pathways, for instance stimulation via the T cell receptor (anti-CD3, CytoStim™) and IFN-α induced broad activation signatures including off-target effects across multiple cell types, whereas TNF-α and LPS elicited more specific responses. Ligand-receptor interaction mapping also uncovered the common and distinct intercellular signalling pathways across stimuli. Comparing the stimuli to patient samples enabled identification of specific inflammatory disease features best replicated by each. For example, IFN-α stimulation recapitulated signatures of SLE across cell types, whereas LPS induced SLE-like changes specifically within monocytes. Comparative cell-cell network analysis showed that *in vitro* stimuli were able to recreate some, but not all, aspects of intercellular interactions upregulated in SLE, highlighting the limitations of these model systems. This resource provides new insights into the similarities and differences of established immune stimuli at cellular resolution and facilitates appropriate use of *in vitro* systems to study pathways relevant to disease.

Introduction

Profiling immune cells and their responses to perturbations is a key element in researching diseases such as autoimmunity and cancer. However, access to patient tissues can be challenging logistically and in terms of scale, where low numbers of samples are available but large heterogeneity between patients necessitates large sample sizes. To overcome this, researchers routinely use immune cell activation assays with peripheral blood mononuclear cells (PBMCs), often from healthy donors, as a more accessible and controlled primary cell system to elucidate inflammatory mechanisms and for pre-clinical testing of potential therapeutics with a range of molecular readouts [1]. For example, stimulating immune cells with interferons to reproduce the biology of systemic lupus erythematosus (SLE) [2], with toll-like receptor agonists such as lipopolysaccharide (LPS) as a model of bacterial or viral infection [3], or using TNF-α stimulation to recreate rheumatoid arthritis biology [4]. A standardised, comparable profile of cellular transcriptomic responses to common *in vitro* stimuli would present a valuable resource: providing a detailed understanding of the biological pathways that are shared and distinct across them whilst also highlighting their strengths and limitations as models of disease. Previous studies profiling transcriptional responses to *ex vivo* stimuli have had narrow scope in terms of diversity of cells and/or stimulation conditions. For instance utilising isolated cell types rather than whole PBMCs, e.g. dendritic cells [5], neutrophils [6], monocytes/macrophages [7, 8, 9] or T cells [9, 10, 11]; or profiling multiple cell types but with a single or limited number of conditions, e.g. LPS [12] or anti-CD3/CD28 + IL-2 [13, 14]. With the largest studies extending to the comparison of three stimuli [15, 16]. A larger, recent, study profiled responses across a range of cytokines head-to-head but focused on immune cells from mouse lymph nodes after 4 hours of *in vivo* stimulation [17]. Thus, a comprehensive, comparative, high-resolution map of immune responses across human cell type populations and commonly used *in vitro* stimuli is lacking.

To address this, we applied single cell RNA sequencing (sc-RNA-seq) to profile the responses of healthy donor PBMCs to 11 different immunomodulatory stimuli. These were selected to include common stimuli, both broadly activating and inhibitory, targeting diverse pathways and cell types. Integration of the data across donors and conditions enabled systematic comparisons of the effects of each condition within 21 identified immune cell subtypes, including elucidation of differential cell-cell communication pathways in the mixed-cell system. As an example of the utility of this resource, we compared the stimulation data to transcriptomic data from immune cells sorted from the blood of patients with a range of immune-mediated diseases [18, 19] and identified the *in vitro* stimuli most representative of each indication. Furthermore, focusing on single-cell data from SLE patients, we identified specific cell-cell interactions enriched in disease and how they are (and are not) recapitulated by different stimuli. These results provide a high-resolution reference of the transcriptional effects of commonly used immunomodulatory conditions at the cellular level. This serves as a foundation for understanding immune cell dynamics, designing immune activation studies, and exploring the molecular mechanisms underlying immune-mediated disease.

Results

Changes in cellular composition across different *in vitro* stimuli

We treated PBMCs from healthy human donors with anti-CD3 antibody, TGF-β1, IL-1β, IL-4, TNF-α, IL-2, IL-10, IFN-α, LPS, CytoStim™, or a B cell stimulator cell line (BCS) expressing CD40L and an anti-CD79B construct (Fig. 1a). The experiment was performed by splitting the stimulation conditions into two batches with 6 donors profiled in each (for a total of 12 unique individuals). After 48 hours, baseline (untreated) and post-treatment samples were profiled by sc-RNA-seq. We identified 21 immune cell subtypes across 153,443 cells (Fig. 1b). Condition- and donor-specific clustering effects were removed for the purposes of annotation only, based on canonical marker expression (Supplementary Fig. 1a and b).

Before detailed analyses of the sc-RNA-seq profiles, we validated them against cell marker expression (Fig.1c) and cell frequencies (Fig. 1d) assessed using flow cytometry. High-level immune cell frequencies were significantly correlated between technologies (Fig. 1d). Anti-CD3 and CytoStim™ treatment induced upregulation of established flow cytometry activation markers, particularly in $CD4^+$ and $CD8^+$ T cells (Fig.1e). Inhibitory conditions such as IL-4, IL-10, and TGF-β1 reduced activation marker expression (e.g., CD38, CD25) in monocytes, while LPS suppressed antigen presentation associated HLA-DR and CD86 expression as previously described [20]. These protein expression measurements were significantly positively correlated with their cognate mRNAs in sc-RNA-seq (Fig. 1c). Discrepancies between technologies were only noted for PD-1 (PDCD1), which exhibited low RNA expression reflecting previous observations [21]. Overall, the flow cytometry comparisons showed good alignment of activation marker and cell type composition with sc-RNA-seq data.

Analysis of cell type composition in the sc-RNA-seq showed monocytes were the most abundant cell type, representing ~30% of cells (Supplementary Fig. 1c). Using more finely grained cell type annotations, we observed overall differences in post-treatment cellular composition across stimuli (Fig. 1f) and inter-donor variability (Supplementary Fig. 1d). Applying compositional statistical analysis, CytoStim™ and anti-CD3 conditions had the highest number of significant proportional shifts, with 6 cell types altered in each (Supplementary Fig. 1e). The profiles resulting from these treatments were largely similar, with reduced naïve $CD4^+$ and $CD8^+$ T cells and a corresponding increase in proliferating T cells (driven to the greatest extent by CytoStim™). However, anti-CD3 treatment also increased the proportion of proliferating B cells, an effect not observed with CytoStim™. An increase in proliferating T cells was also driven by the IL-2 and TGF-β1 treatments.

Myeloid proportions were affected by a range of conditions, particularly conventional dendritic cells (cDCs), which were increased with CytoStim™, anti-CD3, IFN-α and LPS treatment but reduced by IL-10. Plasmacytoid dendritic cell (pDC) abundance was reduced with CytoStim™, LPS and BCS. The BCS stimulation was the only condition in which monocytes were significantly increased. BCS also caused the greatest increase in proliferating B cells as expected. Notably, two conditions (TNF-α and IL-1β) did not induce any significant changes in cell type composition.

Given most changes in cell abundance were in proliferating cell populations, we also examined patterns of cell cycle phase in high level cell type annotations (Supplementary Fig. 1f). As expected, signatures of cell cycle progression were higher in T cells with the T cell-targeted (anti-CD3 and CytoStim™) stimuli, but also to some extent with BCS; whilst B cells were strongly shifted to S-phase by the BCS condition. A strong shift to S-phase was also induced by IL-2 treatment in the ILCs, while IL-4 induced a shift from G2M to G1 phase in B cells. These results highlight that different stimuli induce distinct changes in cell type

composition over 48 hours of culture, which will influence the dominant biology represented by these systems.

Cell types display distinct transcriptional responses to stimuli

Next, we evaluated the magnitude of transcriptional responses elicited by each stimulation on each cell type. Anti-CD3 and CytoStim™ induced widespread transcriptional activation in T cells as expected but also in B and myeloid cells (Fig. 2a). The CytoStim™ treatment, which binds both T cell receptor and MHC molecules on antigen-presenting cells, elicited a larger effect in monocytes and cDCs compared to anti-CD3, which engages the T cell receptor of T cells and Fc receptors of myeloid populations. Conversely, inhibitory conditions such as TGF-β1 and IL-10 reduced gene expression in T cells and monocytes. However, IL-10 uniquely upregulated a small subset of genes in cDCs, while TGF-β1 increased gene expression in mucosal-associated invariant T (MAIT) cells and regulatory T cells (Tregs).

Examining the most altered genes in each cell type-stimulation combination, we observed both cell type-specific and independent changes (Fig. 2b and Supplementary Fig. 2a). For example, IFN-α increased expression of LAMP3 broadly across all cell types, whereas CXCL10 was most elevated in cDCs, central memory $CD4^+$ T cells and memory B cells. CytoStim™ increased IDO1 in B cells and monocytes, whereas SLC16A10 was upregulated only in monocytes. The top genes altered with IL-10 had reduced expression across cell types and included a decrease in the interferon signature genes IFI44L and IFI44. The expression of BCL2, which blocks programmed cell death [22], was most strongly upregulated in T and NK cells in response to IL-2.

To explore broader transcriptional changes, we compared differentially expressed gene (DEG) sets across cell types within each condition (Fig. 2c). This revealed that, for a given stimulation, cell type-specific DEGs were more numerous than those shared between cell

types. This was particularly apparent in myeloid cells, which had a high number of unique DEGs in almost all conditions. However, some similarity in responses was seen across cell types. For example, myeloid and B cells stimulated with BCS shared overlapping DEGs. Thus, whilst there are a small number of stimulation-induced transcriptional responses that are conserved across cell types, such as the IFN gene signature (Fig. 2b), the wider transcriptional signature is largely unique to cell types within a stimulus.

Performing the opposite contrast – comparing DEG signatures between different stimuli (Fig. 2d) – highlighted similarities in transcriptional responses. Considering all cells, positive correlations were observed between IFN-α, LPS and CytoStim™, which were in turn negatively correlated with the inhibitory conditions TGF-β1, IL-4, and IL-10. This pattern was broadly replicated when comparing DEGs within individual cell types; with some key distinctions, for example in the myeloid cells where anti-CD3 stimulation showed strong similarity to CytoStim™, but lacked the inverse correlations to TGF-β1, IL-4, and IL-10. To expand on this finding, we identified a set of genes upregulated by CytoStim™ but not by anti-CD3 in myeloid cells, that were also downregulated by IL-4, IL-10 and TGF-β1 (Fig. 2e). This included interferon signature genes (e.g. ISG15, IFIT3, IFI44L) and the cytokine IL-6. This likely reflects direct myeloid MHC engagement by CytoStim™ that is absent using anti-CD3.

To explore the functional effects of stimuli, we clustered variable genes to identify shared/distinct pathways across cell type-stimulation combinations (Supplementary Fig. 2b). IFN-α stimulation increased interferon pathway expression broadly across cell types, and this was also seen in T cells and ILCs stimulated with anti-CD3 and CytoStim™. A reduction in these activation pathways was observed with IL-4 and IL-10 treatment in myeloid cells, and with TGF-β1, IL-10 and IL-4 treatment in ILCs and T cells. BCS elevated immune cell activation, IL-4, and IL-13 signalling pathways and proliferation pathways in B cells, albeit to a lesser extent than in T cells treated with CytoStim™. Overall, our results demonstrate a

mixture of distinct and overlapping transcriptional responses across stimuli within cell types but largely unique responses between cell types.

Identification of stimulation-specific transcriptional regulation

We explored transcription factor (TF) and target gene enrichment to identify drivers of the observed transcriptional changes. To validate the approach we compared cell types at baseline and observed expected lineage- and cell type-specific patterns (Fig. 3a), including FOXP3 in regulatory T cells [23] and GATA2 in basophils [24]. Interestingly, there was some evidence of pro-inflammatory regulation in the baseline condition with STAT4 [25] target enrichment in NK, MAIT, and effector memory $CD4^+$ T cells, which may reflect response to 48 hours of culture. Comparing the most variable TFs across both cell types and stimulation conditions highlighted stimulation-responsive effects (Fig. 3b). TF target enrichment was broadly split by stimulatory and inhibitory conditions, for example IRF8 and IRF1 target genes were positively enriched by IL-2, anti-CD3, CytoStim™ and IFN-α stimulation, and negatively enriched by IL-4 and TGF-β1. Examining specific TF enrichments in more detail, expression of IRF1 target genes was associated with IFN-α and LPS treatment in nearly all cell types (Fig. 3c). However, more cell type/stimulation-specific TF target gene induction was observed with STAT6, which was notably highest in proliferating T cells after IL-2 treatment but broadly increased across cell types with IL-4 treatment (Fig. 3c). We saw positive correlations between mRNAs for activating TFs (including IRF1 and STAT4) with their downstream genes, and the converse negative associations for repressive TFs (such as HDAC4 and AEBP2) indicating that in these cases changes in target gene enrichment likely reflect changes in TF expression. Finally, we sought out TF regulation unique to specific cell type/condition pairs (Fig. 3e). This included ZBT49, which was enriched in CD56-bright NK cells treated with CytoStim™, and an increase in the target genes of ZNF626 in monocytes responding to IL-4, amongst others.

Differences in cell-cell communication networks between stimuli

We next explored how different stimuli influence the intercellular communication between cell types and might induce the secondary effects observed on non-target cells. Upregulated ligand-receptor interactions between cell types were predicted per condition and compared (Fig. 4a and Supplementary Fig. 3a). Of the 11 stimuli, 8 could be classified into three groups based on the similarity of cell signalling landscapes: BCS and LPS (group 1); IL-2, anti-CD3 and CytoStim™ (group 2); and IL-1β, TNF-α and TGF-β1 (group 3). Group 1 was characterised by signalling into B cells via CD22 from $CD8^+$ T cells and NK cells, group 2 by a dominant signalling from monocytes via IL-15, and group 3 by shared dominance of interactions involving naïve $CD8^+$ T cells (Fig. 4b). Exploring the interaction network of each stimulation individually, we also identified stimulation-specific cell type interactions (Supplementary Fig. 3b). For instance, NOG-BMPR2 binding between $CD4^+$ T cells and NK cells stimulated with TGF-β1, and IL27-IL27RA interactions between IFN-α-stimulated T cells and monocytes. As a more global overview, we highlighted the top 50 upregulated ligand-receptor interactions per condition (Supplementary Fig. 3c). As expected, the cell-cell interaction network for CytoStim™ stimulation includes well-known binding partners between T cells and antigen-presenting cells (B cells, monocytes and DCs), such as CD80 and CD274 on monocytes interacting with CTLA4 and PDCD1 on T cells. Treatment with CytoStim™ also leads to an upregulation of FASLG on NK cells and FAS expression on regulatory T cells, and of IL-15 from B cells interacting with T cells.

We provide a more detailed comparison of these networks for the IFN-α and TGF-β1 conditions, given their generally opposing effects and diverse networks (Fig. 4c and Supplementary Fig. 3d-e), and show the expression data for receptors, ligands, and their downstream pathway genes at the donor level for unique interactions (Fig. 4d). Monocyte IL27 and T cell IL27RA expression were elevated in IFN-α treatment and reduced with TGF-β1, which was reflected in downstream target gene expression in the T cells. One of the most

prominent cell-cell interactions in IFN-α-stimulated cells was BST2 in T cells and B cells interacting with LILRB3 on monocytes. The distinct expression profiles of BST2 and LILRB3 at the mRNA level (Fig. 4e) highlighted that LILRB3 remained constitutively expressed in monocytes, but BST2 was upregulated in central memory $CD4^+$ T cells, NK cells and B cells with IFN-α treatment. Key signalling induced by TGF-β1 included: increased ENG in monocytes, which communicates via BMPR2 on B cells and ITGAV on NK cells and monocytes (auto-regulatory), and the production of TGF-βI by monocytes that can interact with integrins ITGA5 and ITGA1 expressed on NK cells [26]. These intercellular pathways were associated with expected intracellular transcriptional differences when comparing IFN-α and TGF-β1 directly, with IFN-α stimulating interferon pathways that were suppressed by TGF-β1 and clear activation of TGF-β pathways with TGF-β1 (Fig. 4f). These inter cell-type interactions may represent key targets to interrupt activation cascades within mixed-cell populations.

Identifying aspects of disease biology reproduced by *in vitro* stimuli

To assess how the stimuli reflect disease biology, we compared their transcriptomic signatures and cell-type interaction networks to those derived from patients with immune-mediated disease. First, we compared stimulation-cell type transcriptomic signatures to those derived from bulk RNA-seq of cell types sorted from PBMCs from 10 different inflammatory diseases in the ImmuNexUT cohort[19] (Supplementary Fig. 4a). Broadly, genes upregulated in disease were positively enriched with activating stimuli (IL-2, BCS, anti-CD3, LPS, IFN-α, and CytoStim™) and reduced with immunosuppressive conditions (TGF-β1, IL-10, IL-4 and TNF-α). However, certain diseases were poorly correlated across most stimuli including ANCA-associated vasculitis and Takayasu arteritis. Certain stimuli were also more highly correlated with specific diseases. For example, focusing on RA, SLE and systemic sclerosis (SSc) (Fig. 5a), *in vitro* IFN-α treatment was highly correlated across all three conditions, whereas CytoStim™ and LPS showed greater overlaps with SLE than with RA or SSc.

Notably, most stimuli showed consistent enrichments with disease signatures (either positive, poor, or negative) across all cell types.

To demonstrate the utility of our stimulation data for more detailed comparative analyses at the cellular level we chose to focus on a sc-RNA-seq dataset from patients with SLE - a disease with established peripheral inflammatory signatures that correlated with several *in vitro* stimuli in the prior bulk RNA-seq analyses. We reannotated published single-cell RNA-seq data from PBMCs of SLE patients and healthy donors to facilitate direct comparison to our in *vitro* stimuli (Fig. 5b, Supplementary Fig. 4b-c)[18]. SLE signatures were most closely reproduced by CytoStim™ and IFN-α stimuli across most cell types, but with distinct patterns between the two (Fig. 5c). Other conditions show more limited, cell type-specific upregulation of SLE associated genes, such as in LPS stimulation of monocytes. Interestingly, while MAIT cells were extensively transcriptionally altered in SLE (n DEGs = 3,781; Supplementary Fig. 4d), an effect previously observed in circulating MAIT cells from SLE patients [27], this was not reproduced by any *in vitro* stimulation. This contrasts with monocytes, in which transcriptional changes highly similar to SLE were induced by multiple stimuli.

We then compared the network of inter-cell type interactions enriched in SLE to those induced by different stimuli (Fig. 5e). Many of the dominant signalling pathways in SLE were also enriched in the IFN-α stimulated PBMCs (Fig. 4c), such as BST2-LILRB3 between monocytes and T cells. Furthermore, when comparing the global cell type interaction network of SLE to each stimulation (Fig. 5d), IFN-α had the highest overlap to the SLE network. However, whilst the IFN-α and SLE networks shared many overlapping edges, unique interactions were also enriched in each (Fig. 5f). The SLE network uniquely included B cells interacting with monocytes (via CD69-S100A8) – this may indicate pathways upstream of IFN production not recapitulated by IFN-α *in vitro*. Conversely, IL-27 signalling was prevalent in the IFN-α stimulation network but absent in SLE.

Comparative analyses reiterate the value of *in vitro* stimulation systems as models of human disease, but also the need to understand the limits of their representation.

As a final comparison with alternate model systems, we explored the similarity of our *in vitro* signatures to those from *in vivo* models recently described in the Immune Dictionary dataset [17] (Supplementary Fig. 4e-f). This study assessed effects of cytokines 4 hours after administration in mice. The largest overlap between our *in vitro* data and *in vivo* effects (in terms of number of DEGs) was observed across all cell types after IFN-α treatment (Supplementary Fig. 4e). However, in general, the overall extent of transcriptional shifts in the murine cytokine treatments was much smaller than in our *in vitro* system (Supplementary Fig. 4f), and there was low and, in some cases, negative correlations between them. This is not unexpected given the species, tissular, and protocol differences between the data sets and reiterates the necessity to understand how representative model systems are of the desired biology.

Discussion

This study provides a foundational resource for understanding immune responses to a variety of typical *in vitro* stimuli, providing insights into both their direct and indirect effects within a mixed immune cell population, and how closely these reproduce disease relevant biology. We found that whilst certain stimuli can have similar effects on specific cell types, for instance the effect of anti-CD3, CytoStim™ and IL-2 on T cells, there is relatively little overlap in the transcriptional changes to any given stimuli across different cell types. The relative magnitude and specificity of effects also varied between conditions. For example, CytoStim™, and IFN-α both induced large transcriptional changes in T cells but also in multiple other cell lineages, where as anti-CD3 or TNF-α would be more appropriate stimuli to limit effects to the T cell populations. The largest transcriptional divergence was, as expected, between the immunosuppressive effects of TGF-β1, IL-10 and (in monocytes) IL-4 and the activating conditions. Although notably the $CD8^+$ T cell signatures for patients with immune disease positively correlated with IL-4-induced changes on $CD8^+$ T cells, highlighting a complexity beyond a simple activating vs. inhibitory framework.

Ligand-receptor interaction analysis revealed key mechanisms of inter-cell type communication. For example, IFN-α stimulation induced IL27 production by monocytes, which was predicted to act on T cells via the IL27RA receptor. This is consistent with the role of IL-27 in autoimmune regulation, where response of T cells to IL-27 leads to an increase in the anti-inflammatory cytokine IL-10, inhibition of T-helper 17 cell differentiation, and subsequent inhibition of IL-17 [28]. IL-27 has been implicated in inflammatory and autoimmune-related diseases, such as inflammatory bowel disease, where it is likely involved in an inadequate anti-inflammatory response [29]. TGF-β1 treatment modulated myeloid-B cell interactions through the upregulation of ENG and BMPR2, which can impact B cell maturation and long-term humoral immunity [30, 31]. These findings align with prior studies demonstrating the immunoregulatory effects of these cytokines [32]. The ligand-receptor

interaction analysis also identified more complex networks, such as the upregulation of BST2 in IFN-α-stimulated T and B cells, which interacted with LILRB3 on monocytes. BST2 has been implicated in type I interferon signalling and autoimmune diseases such as SLE [18]. While these results are inherently limited by the quality and completeness of interaction databases, they provide a mechanism to uncover the key signalling pathways within immune cell networks, which may prove promising targets for immunomodulation.

Evaluation of TF targets also identified several key regulators of immune response within and across cell types. IRF1, an established TF downstream of IFN signalling [33], regulation was elevated with IFN-α but also with IL-2, CytoStim™, anti-CD3, and reduced by inhibitory stimuli (IL-10, IL-4 and TGF-β1). This suggests indirect signalling via IFNs was common across stimuli. IL-4 increased STAT6 target gene expression across multiple cell types [34], whereas this was limited to proliferating T cells when treating with IL-2; a pathway previously associated with T cell functionality in autoimmunity [35]. We also identified TFs specific to unique stimulation-cell type combinations. ZBT49 regulation was enriched in NK cells treated with CytoStim™ and has been previously linked to their cytotoxic potential [36]. Monocytes treated with IL-4 had increased expression of genes regulated by ZNF626, previously associated with macrophage M2 polarisation [37]. Similar profiling of alternate regulators of transcription, such as small and other non-coding RNAs, at the single-cell level could uncover further novel controls influencing immune response.

An important goal of this study was to evaluate how well *in vitro* stimuli recapitulate immune diseases and *in vivo* systems. Comparing our data to *in vivo* mouse cytokine response data from the "Immune Dictionary" [17] showed that IFN-α responses were highly conserved across both, particularly in myeloid and T cells. However, discrepancies were noted for all other cytokines tested in both, such as IL-2 and TGF-β1. This highlights the complementary value of *in vitro* and *in vivo* models and the need for comprehensive profiling of these systems. Divergence between these data sets was not unexpected given the difference in their

experimental approaches including cell culture, durations of stimulation, and species. Better alignment between *in vitro* and *in vivo* data might be expected if using mice with humanised leukocytes, which can respond similarly to *in vitro* PBMCs albeit with some differences [38].

Comparing the *in vitro* stimuli to patient data showed that multiple stimuli reproduce transcriptional changes observed in immune mediated disease. As expected, IFN-α upregulated SLE-relevant genes including BST2 across multiple cell types. Conversely, inhibitory conditions like TGF-β1 and IL-10 downregulated SLE disease activation signatures, consistent with their roles as anti-inflammatory mediators. The type 1 interferon stimulated gene response in SLE is well documented across many cell types, with both functional changes in monocytes and compositional changes in the $CD4^+$ T cell compartment [2, 18, 39]. Identifying key interactions between disease-associated cells in this context could offer new avenues of therapeutic intervention. Comparing networks, we found high similarity between SLE and *in vitro* IFN-α, LPS and anti-CD3 stimuli suggesting these accurately recapitulate between cell-type interactions that are elevated in SLE. However, our analyses also highlighted molecular changes in SLE that were not recreated by any *in vitro* stimulation, such as transcriptional shifts in peripheral MAIT cells, which reflects a poor representation of peripheral biology sourced from diseased tissue. The use of *in vitro* stimuli as models of disease necessitates a thorough understanding of both disease and model biology to select appropriate systems to represent the disease state of individual patients. Further exploration of additional cytokines, pathogen-associated molecular patterns [40, 41], or co-stimulatory molecule combinations [42, 43], will aid this.

The single cell profiles of PBMC responses to *in vitro* stimuli presented here expand our understanding of immune cell dynamics by enabling the identification of condition-specific effects on cell type composition, intracellular transcriptional regulation, and intercellular communication. Furthermore, it provides a resource to assess the relevance of *in vitro* models

to recapitulate key features of human disease. Together these features provide a foundation for accelerating immunological research and the development of immune-targeted therapies.

Methods

Sample collection and *in vitro* stimuli

Blood cones were processed to obtain PBMCs using density gradient centrifugation. Briefly, diluted blood cone cells were layered over Ficoll-Paque PLUS Media (Cytiva) in a 50 mL Leucosep tube (Greiner Bio-One GmbH). The resulting cells were seeded into tissue culture treated Biolite 24-well plates (Thermo Fisher scientific) at a density of $1x10^5$/ cm^2 in a final volume of 1 mL of RPMI (Gibco), supplemented with Penicillin-Streptomycin-Neomycin (Gibco), 10% Foetal Bovine Serum (Gibco) and L-Glutamine (Gibco). A total of 12 separate donors were used, with stimulations carried out across 2 phases with each batch having 6 different donors and a baseline condition. The stimulation conditions used were 1 ng/mL Ultra-LEAF Purified anti-human CD3 antibody, 10 ng/mL human TGF-β1, 1 ng/mL GMP Human IL-1β, 10 ng/mL human IL-4 GMP, 10 ng/mL human TNF-α GMP, 10 ng/mL human IL-2 GMP, 10 ng/mL human IL-10 GMP, human IFN-α (Biolegend), 100 ng/mL lipopolysaccharide (LPS) solution (eBiosciences), 20 µl/mL CytoStim™ human (Miltenyi Biotec), and the B cell stimulator cells (8:1, PBMC:BCS) with 100 ng/mL IL-21 (Biolegend). Concentration gradients for each stimulation were performed in pilot experiments to establish optimal concentrations to maximise stimulation (as assessed using common markers by flow cytometry) at 48 hours whilst minimising death of cell populations (Supplementary Fig. 5). The B cell stimulator cells consisted of HEK293 (ATCC) cells transduced to express CD40L and an anti-CD79B ScFv construct. These were seeded at a density of $1x10^5$/ cm^2 the day prior to the experiment and were grown in Dulbecco's Modified Eagle Medium (DMEM) supplemented with Penicillin-Streptomycin-Neomycin (Gibco), 10% Foetal Bovine Serum (Gibco) and L-Glutamine (Gibco).

Flow cytometric evaluation

Following the *in vitro* stimulation, $2x10^5$ of the harvested cells were used to determine the cell proportions and activation readouts using fluorescent activated cell sorting (FACS) on the BD FACSAria™ Fusion. The activation readouts were captured with cell surface staining for CD38 (HIT2), CD25 (MA251), HLA-DR (L243), CD86 (FUN-1) and PD-1 (EH12.2H7). The cell markers for lineage determination and cell proportion analysis were CD8 (SK1), CD14 (M5E2), CD19 (HIB19), CD56 (5.1H11) CD3 (HIT3a) and CD4 (OKT4). Live cells were gated using DAPI (4',6-diamino-2-phenylindole, dihydrochloride) staining solution (Miltenyi Biotec).

Single cell library preparation and sequencing

Harvested cells from the *in vitro* stimulation were fixed using the Evercode™ cell fixation kit v2 (Parse Biosciences) according to the manufacturer's protocol. The average yield of fixed cells taken forward to SPLiT-seq (split-pool ligation-based transcriptome sequencing) was $5x10^5$. The library preparation and sequencing were carried out using the Evercode™ WT 100k whole transcriptome kit v2 (Parse Biosciences) according to the manufacturer's protocol. The initial fixed cell samples were counted using a Countess 3 (Thermo Fisher Scientific) cell counter to achieve 100,000 cells/barcode. After barcoding, eight sub-libraries were prepared, each containing ~10,000 cells. The final libraries underwent standard library QC and quantification followed by sequencing on 2x NovaSeq X Plus (Illumina) 25b 300 cycle Flow Cell Lanes, set to 150bp paired-end read mode. The demultiplexed fastQ files were processed though the Parse pipeline (v1.2.1) and used for the following processes: demultiplexing, trimming, filtering and alignment of reads to reference (GRCh38); assignment of reads to cell barcodes; per-sample QC and filtering of cells vs. ambient RNA; output of filtered count matrices for downstream analyses.

Single cell transcriptomic profiles

Single cell transcriptomic profiles were processed using Seurat (v5.1.0) [44] in R. Low complexity/unhealthy cells were removed as defined by >15% mitochondrial UMIs or <=0.8 log10-genes per UMI. Genes with zero detected counts across all cells were removed. Preliminary, per-cell automated cell type prediction was performed with Singler (v2.4.1) [45] using a sorted PBMC bulk RNA-seq reference dataset [46]. Doublet Finder (v2.0.4) [47] was used to remove predicted multiplets by comparing the gene expression profile of each cell to *in silico* generated multiplet profiles based on Singler annotations, with an assumed multiplet rate of 3%. An initial UMAP dimensional reduction and clustering was performed (resolution = 0.50, first 30 principle components based on 3000 variable genes), this enabled the removal of the remaining B cell stimulator cells. Cell cycle and batch effects on final cell clustering and annotation were minimised by were integrating across samples with reciprocal PCA [48]. Using baseline samples as a reference, the first 30 principal components based on a consensus set of 4000 variable genes across samples determined by the variance stabilising transformation method, with cell cycle genes excluded, and variable genes scaled while regressing out total RNA count and percentage mitochondrial UMIs. Post-integration UMAP dimensional reduction and clustering were performed (resolution = 1.4) for visualisation and to assign lineage labels (T/ILC, B, myeloid), then cells were re-clustered separately within each lineage at multiple resolutions (0.2, 0.4, 0.6, 0.8, 1.0). Within each lineage, the expression patterns of relevant marker genes were assessed per cluster to inform selection of final resolutions per lineage (T/ILC, 0.4; B, 0.2; myeloid, 0.4) and assign cluster IDs based on the chosen clustering. Differentially expressed genes were determined per cluster vs. all other clusters using a Wilcoxon Rank Sum test and cell types annotated based on the top marker genes per cluster. Finally, low quality and suspected doublet/mixed clusters were removed from downstream analyses.

Assessment of cell type- and condition-specific effects

Differential cell type compositional analysis was performed using Propeller [49] comparing each condition to baseline, with donor adjusted as a mixed effect. Aggregated pseudo-bulk transcriptomic profiles were generated per cell type (separately at the general and subtype level as appropriate), condition, and donor. Pseudo-bulk profiles were used to calculate differentially expressed genes per cell type (either vs. all other cells in the baseline condition, for cell type-specific genes; or for each condition vs. baseline, for stimulation-responsive genes) with DESeq2 (v1.42.1) [50] while adjusting for donor effects. DEGs were defined by adjusted $p<0.05$ unless a different stringency threshold or additional criteria (such as log2-fold change) were required for specific analyses (and are stated as such). Comparisons of the altered transcriptomic profiles within and between datasets were summarised by the following metrics, where appropriate: Jaccard index of DEGs, defined as the ratio of the intersect size to the union size; correlation of log2-fold changes, using Pearson correlation unless otherwise stated; normalised enrichment score (NES) from gene set enrichment analysis of gene positions within gene profiles ranked by Wald statistic (log2-fold change divided by standard error of log2-fold change) with the fgsea package (v1.28.0) [51]. Functional annotation of DEG profiles was also performed by over-representation analysis of DEGs ($p<0.05$) compared to universe (all detected genes) using fgsea with Reactome pathway annotations of size 30-300[52]. MultiNicheNet [53] (v2.0.1) was used to assess cell-cell communication comparing cells from each condition to baseline, with donor as a covariate and the following options: min_sample_prop = 0.50; fraction_cutoff = 0.05; empirical_pval = FALSE; logFC_threshold = 1.5; p_val_threshold = 0.05; p_val_adj = FALSE; top_n_target = 250. Interaction edge lists produced by multiniche net were converted to networks for each stimulation selecting the top 2000 edges based on the MultiNicheNet prioritisation score. This threshold was selected by generating networks with increase numbers of edges and comparing the overlap between conditions to find a size with enough edges that similarities

and differences between conditions could be observed but not so many that the networks became homogenous (Supplementary Fig. 3a).

Additional datasets

Gene count matrices from sorted bulk RNA-seq profiles from the ImmunexUT study [19] were obtained from the National Bioscience Database Center (NBDC) Human Database (accession E-GEAD-397). Cell type-specific DEG profiles ($p<0.01$, log2-fold change > 0.5) for each disease vs. healthy were generated using LIMMA [54]. Sc-RNA-seq profiles from SLE and normal cells [18] (GSE174188) were obtained as a pre-processed Seurat object from BioTuring [55]. The Seurat anchor-finding and label transfer functionality was used to guide reannotation of the SLE/normal cells using labels from the *in vitro* stimulated PBMCs, with some manual adjustment of cell annotations where appropriate. DEGs were assessed per cell type as SLE vs. normal cells with the pseudo-bulk DESeq2 method as previously used. Ligand-receptor interactions were assessed with the MultiNicheNet method as previously used, but without using donor as a covariate (as groups were mutually exclusive in this dataset). Sc-RNA-seq profiles from mice treated with cytokines [17] (GSE202186) were obtained as pre-processed Seurat objects from the authors. DEGs were assessed per cell type as cells from treated vs. untreated mice with the Wilcoxon rank sum test ($p<0.05$). Mouse gene symbols were converted to human gene symbols based on 1:1 orthologs as determined via NCBI HomoloGene [56] and biomaRt [57]. Differential gene profiles for human PBMC stimuli vs. baseline were generated for cells with matching annotation levels (B cell, NK cell, $CD4^+$ T cell, $CD8^+$ T cell, regulatory T cell, cDC1, cDC2 and pDC) to the available mouse data using a similar cell-level Wilcoxon rank sum test ($p<0.05$).

Acknowledgments

We sincerely thank Dr Sara Silva and Liam Hardy for generating the B cell stimulator cell line.

Data availability

Code and raw data will be made available on publication, current version of processed data can be found here: https://doi.org/10.5281/zenodo.15744698.

Contributions

O.W., A.T.B, M.JW. conceived of the work. O.W, A.T.B, M.JW, J.F, L.M, C.P, L.L contributed to experiment and analytical design. O.W., A.T.B. and M.JW performed data analysis and wrote the manuscript. O.W performed the cell isolations and *in vitro* experimentation. All authors provided feedback on the manuscript.

References

1. Kleinstreuer NC, *et al.* Phenotypic screening of the ToxCast chemical library to classify toxic and therapeutic mechanisms. *Nat Biotechnol* **32**, 583-591 (2014).

2. Pascual V, Farkas L, Banchereau J. Systemic lupus erythematosus: all roads lead to type I interferons. *Curr Opin Immunol* **18**, 676-682 (2006).

3. Duan T, Du Y, Xing C, Wang HY, Wang RF. Toll-Like Receptor Signaling and Its Role in Cell-Mediated Immunity. *Front Immunol* **13**, 812774 (2022).

4. Jang DI, *et al.* The Role of Tumor Necrosis Factor Alpha (TNF-alpha) in Autoimmune Disease and Current TNF-alpha Inhibitors in Therapeutics. *Int J Mol Sci* **22**, (2021).

5. Reyes M, Leff SM, Gentili M, Hacohen N, Blainey PC. Microscale combinatorial stimulation of human myeloid cells reveals inflammatory priming by viral ligands. *Sci Adv* **9**, eade5090 (2023).

6. Montaldo E, *et al.* Cellular and transcriptional dynamics of human neutrophils at steady state and upon stress. *Nat Immunol* **23**, 1470-1483 (2022).

7. Wendisch D, *et al.* SARS-CoV-2 infection triggers profibrotic macrophage responses and lung fibrosis. *Cell* **184**, 6243-6261 e6227 (2021).

8. Fairfax BP, *et al.* Innate immune activity conditions the effect of regulatory variants upon monocyte gene expression. *Science* **343**, 1246949 (2014).

9. van der Heijden WA, *et al.* Chronic HIV infection induces transcriptional and functional reprogramming of innate immune cells. *JCI Insight* **6**, (2021).

10. Cano-Gamez E, *et al.* Single-cell transcriptomics identifies an effectorness gradient shaping the response of CD4(+) T cells to cytokines. *Nat Commun* **11**, 1801 (2020).

11. Szabo PA, *et al.* Single-cell transcriptomics of human T cells reveals tissue and activation signatures in health and disease. *Nature Communications* **10**, 4706 (2019).

12. Derbois C, Palomares MA, Deleuze JF, Cabannes E, Bonnet E. Single cell transcriptome sequencing of stimulated and frozen human peripheral blood mononuclear cells. *Sci Data* **10**, 433 (2023).

13. Mimitou EP, *et al.* Scalable, multimodal profiling of chromatin accessibility, gene expression and protein levels in single cells. *Nat Biotechnol* **39**, 1246-1258 (2021).

14. Lawlor N, *et al.* Single Cell Analysis of Blood Mononuclear Cells Stimulated Through Either LPS or Anti-CD3 and Anti-CD28. *Front Immunol* **12**, 636720 (2021).

15. Kartha VK, *et al.* Functional inference of gene regulation using single-cell multi-omics. *Cell Genom* **2**, (2022).

16. Oelen R, *et al.* Single-cell RNA-sequencing of peripheral blood mononuclear cells reveals widespread, context-specific gene expression regulation upon pathogenic exposure. *Nat Commun* **13**, 3267 (2022).

17. Cui A, *et al*. Dictionary of immune responses to cytokines at single-cell resolution. *Nature* **625**, 377-384 (2024).

18. Perez RK, *et al*. Single-cell RNA-seq reveals cell type-specific molecular and genetic associations to lupus. *Science* **376**, eabf1970 (2022).

19. Ota M, *et al*. Dynamic landscape of immune cell-specific gene regulation in immune-mediated diseases. *Cell* **184**, 3006-3021.e3017 (2021).

20. Wolk K, Do□cke W-D, von Baehr V, Volk H-D, Sabat R. Impaired antigen presentation by human monocytes during endotoxin tolerance. *Blood* **96**, 218-223 (2000).

21. Fisher J, Wood O, Bullers S, Murray L, Li L, Jackson-Wood MA. Machine Learning Predictions Surpass Individual mRNAs as a Proxy of Single-cell Protein Expression. *bioRxiv*, 2024.2012.2011.627925 (2024).

22. Korsmeyer SJ. BCL-2 gene family and the regulation of programmed cell death. *Cancer Res* **59**, 1693s-1700s (1999).

23. Rudensky AY. Regulatory T cells and Foxp3. *Immunol Rev* **241**, 260-268 (2011).

24. Li Y, Qi X, Liu B, Huang H. The STAT5-GATA2 pathway is critical in basophil and mast cell differentiation and maintenance. *J Immunol* **194**, 4328-4338 (2015).

25. Yang C, Mai H, Peng J, Zhou B, Hou J, Jiang D. STAT4: an immunoregulator contributing to diverse human diseases. *Int J Biol Sci* **16**, 1575-1585 (2020).

26. Bissey PA, *et al*. Dysregulation of the MiR-449b target TGFBI alters the TGFbeta pathway to induce cisplatin resistance in nasopharyngeal carcinoma. *Oncogenesis* **7**, 40 (2018).

27. Chiba A, *et al*. Activation status of mucosal-associated invariant T cells reflects disease activity and pathology of systemic lupus erythematosus. *Arthritis Res Ther* **19**, 58 (2017).

28. Batten M, Kljavin NM, Li J, Walter MJ, de Sauvage FJ, Ghilardi N. Cutting edge: IL-27 is a potent inducer of IL-10 but not FoxP3 in murine T cells. *J Immunol* **180**, 2752-2756 (2008).

29. Andrews C, McLean MH, Durum SK. Interleukin-27 as a Novel Therapy for Inflammatory Bowel Disease: A Critical Review of the Literature. *Inflamm Bowel Dis* **22**, 2255-2264 (2016).

30. Lastres P, *et al*. Endoglin modulates cellular responses to TGF-beta 1. *J Cell Biol* **133**, 1109-1121 (1996).

31. Tomayko MM, *et al*. Roles of Bone Morphogenetic Protein Receptor 1A in Germinal Centers and Long-Lived Humoral Immunity. *Immunohorizons* **5**, 284-297 (2021).

32. Akdis M, *et al*. Interleukins (from IL-1 to IL-38), interferons, transforming growth factor β, and TNF-α: Receptors, functions, and roles in diseases. *J Allergy Clin Immunol* **138**, 984-1010 (2016).

33. Man SM, *et al*. The transcription factor IRF1 and guanylate-binding proteins target activation of the AIM2 inflammasome by Francisella infection. *Nat Immunol* **16**, 467-475 (2015).

34. Takeda K, *et al*. Essential role of Stat6 in IL-4 signalling. *Nature* **380**, 627-630 (1996).

35. Kato H, Perl A. Double-Edged Sword: Interleukin-2 Promotes T Regulatory Cell Differentiation but Also Expands Interleukin-13- and Interferon-gamma-Producing CD8(+) T Cells via STAT6-GATA-3 Axis in Systemic Lupus Erythematosus. *Front Immunol* **12**, 635531 (2021).

36. Xu W, *et al.* An Id2(RFP)-Reporter Mouse Redefines Innate Lymphoid Cell Precursor Potentials. *Immunity* **50**, 1054-1068.e1053 (2019).

37. Fan J, Zhang M, Wu H, Ye Z, Wang L. Estrogen Promotes Endometrial Cancer Development by Modulating ZNF626, SLK, and RFWD3 Gene Expression and Inducing Immune Inflammatory Changes. *Biomedicines* **13**, (2025).

38. Cheng L, *et al*. Human innate responses and adjuvant activity of TLR ligands in vivo in mice reconstituted with a human immune system. *Vaccine* **35**, 6143-6153 (2017).

39. Nehar-Belaid D, *et al*. Mapping systemic lupus erythematosus heterogeneity at the single-cell level. *Nat Immunol* **21**, 1094-1106 (2020).

40. Serrano R, Wesch D, Kabelitz D. Correction: Serrano, R.; Wesch, D.; Kabelitz, D. Activation of Human gammadelta T Cells: Modulation by Toll-Like Receptor 8 Ligands and Role of Monocytes. Cells 2020, 9, 713. *Cells* **9**, (2020).

41. Vlaming KE, *et al.* Crosstalk between TLR8 and RIG-I-like receptors enhances antiviral immune responses. *Front Med (Lausanne)* **10**, 1146457 (2023).

42. Fleige L, Capellino S. Simultaneous Stimulation of Peripheral Blood Mononuclear Cells with CpG ODN2006 and alpha-IgM Antibodies Leads to Strong Immune Responses in Monocytes Independent of B Cell Activation. *Cells* **13**, (2024).

43. Glass MC, *et al*. Human IL-10-producing B cells have diverse states that are induced from multiple B cell subsets. *Cell Rep* **39**, 110728 (2022).

44. Hao Y, *et al*. Dictionary learning for integrative, multimodal and scalable single-cell analysis. *Nature Biotechnology* **42**, 293-304 (2024).

45. Aran D, *et al*. Reference-based analysis of lung single-cell sequencing reveals a transitional profibrotic macrophage. *Nature Immunology* **20**, 163-172 (2019).

46. Monaco G, *et al.* RNA-Seq Signatures Normalized by mRNA Abundance Allow Absolute Deconvolution of Human Immune Cell Types. *Cell Rep* **26**, 1627-1640.e1627 (2019).

47. McGinnis CS, Murrow LM, Gartner ZJ. DoubletFinder: Doublet Detection in Single-Cell RNA Sequencing Data Using Artificial Nearest Neighbors. *Cell Systems* **8**, 329-337.e324 (2019).

48. Hao Y, *et al*. Integrated analysis of multimodal single-cell data. *Cell* **184**, 3573-3587.e3529 (2021).

49. Phipson B, Sim CB, Porrello ER, Hewitt AW, Powell J, Oshlack A. propeller: testing for differences in cell type proportions in single cell data. *Bioinformatics* **38**, 4720-4726 (2022).

50. Love MI, Huber W, Anders S. Moderated estimation of fold change and dispersion for RNA-seq data with DESeq2. *Genome Biology* **15**, 550 (2014).

51. Korotkevich G, Sukhov V, Budin N, Shpak B, Artyomov MN, Sergushichev A. Fast gene set enrichment analysis. *bioRxiv*, 060012 (2021).

52. Milacic M, *et al.* The Reactome Pathway Knowledgebase 2024. *Nucleic Acids Res* **52**, D672-D678 (2024).

53. Browaeys R, *et al.* MultiNicheNet: a flexible framework for differential cell-cell communication analysis from multi-sample multi-condition single-cell transcriptomics data. *bioRxiv*, 2023.2006.2013.544751 (2023).

54. Ritchie ME, *et al.* limma powers differential expression analyses for RNA-sequencing and microarray studies. *Nucleic Acids Res* **43**, e47 (2015).

55. Bioturing. B browserX. https://bioturing.com/single-cell-analysis-bbrowserx

56. NCBI. HomoloGene. http://www.ncbi.nlm.nih.gov/homologene

57. Durinck S, Spellman PT, Birney E, Huber W. Mapping identifiers for the integration of genomic datasets with the R/Bioconductor package biomaRt. *Nat Protoc* **4**, 1184-1191 (2009).

Figure legends

Fig. 1 | Creating a map of responses to 11 immunomodulators across 21 immune cell types

(A) Schematic overview of the experimental and computational workflow. (B) UMAP dimensional reduction of 153,443 cells integrated across conditions. (C) Pearson correlation of log2-fold changes (gMFI) from flow cytometry protein measurements vs. log2-fold change normalised counts from sc-RNA-seq data (stimulation vs. baseline) for activation markers. For sc-RNA-seq data, profiles were summarised as mean pseudo bulk profiles per general cell type / stimulation to calculate fold changes vs. baseline. (D) Spearman correlation of broad cell type (B cell, CD4, CD8 and monocytes) frequencies between flow cytometry and single cell RNA-Seq, split by cell type across donors. (E) Altered levels of surface protein activation markers determined by flow cytometry in CD4+ T cells, CD8+ T cells, B cells and monocytes. Mean log2-fold change (gMFI) is shown for each condition vs. baseline. (F) Combined cell proportions from 6 donors per stimulation and 12 donors (2 batches of 6) for baseline. Cell types of >= 1% are labelled. B_mem, memory B cells; B_n, naive B cells; CD4_Tcm, central memory CD4 T cells; CD4_Tem, effector memory CD4 T cells; CD4_Tn, naive CD4 T cells; Treg, T regulatory cells; CD8_CTL, CD8 cytotoxic T cells; CD8_Tm, memory CD8 T cells; CD8_Tn, naive CD8 T cells; MAIT, mucosal-associated invariant T cells; NK, natural killer cells; NK_CD56_br, CD56-bright NK cells; NKT, NK T cells; baso, basophils; cDC, conventional dendritic cells; mono, monocytes; pDC, plasmacytoid dendritic cells; prog, progenitor cells; B_prolif, proliferating B cells; ILC_prolif, proliferating ILC; T_prolif, proliferating T cells.

Fig. 2 | Quantitative comparison of the overall transcriptomic responses.

(A) Transcriptomic changes within pseudo-bulk profiles per cell type comparing each condition to baseline. Number of differentially expressed genes (DEGs; $p<0.05$) and mean log2-fold change (FC) of all DEGs is shown per comparison. (B) Log2-fold changes for top 4

DEGs per lineage (B, T, ILC, myeloid) by lowest p-values, for key stimulations vs. baseline. (C) Specific and shared DEGs per stimulation vs. baseline across general cell types. For overlapping DEG sets, those with >=2000 shared genes in at least 2 general cell types are shown. (D) Similarity of DEG profiles between conditions evaluated by Pearson correlation of FC for all genes and Jaccard similarity index of DEG sets. Comparisons were based on pseudo-bulk DEG profiles from all cells or general cell types. (E) Log2-FC for significant DEGs ($p<0.05$) upregulated by CytoStim™ and downregulated by IL-4, IL-10 and TGF-β1, but not altered by anti-CD3, in myeloid lineage cells.

Fig. 3 | Transcriptional regulation in response to immunomodulation.

Enrichment of transcription factor (TF) target genes (obtained from GTRD and ChEA) within cell type-specific (cell type at baseline vs. other cell types) and stimulation-response (stimulation vs. baseline within a cell type) gene profiles were assessed by gene set enrichment analysis. (A) Log2-fold change (FC) of TF mRNA and normalised enrichment score (NES) of TF target genes is shown for up to 4 top cell type-specific TFs per cell type. Data was filtered to TFs with significant ($p<0.05$) and positive TF mRNA and TF target NES per cell type. (B) The top 50 stimulation-responsive TFs by variance of NES across all cell types and conditions are shown. Each column represents a minor cell type/stim, annotated per general cell type. NES for significant enrichments ($p<0.05$) are highlighted in colour. (C) Example profiles of enrichment for key TF (IRF1 and STAT6) targets across cell types and conditions. (D) Comparison of differential TF expression vs. enrichment of TF target gene expression, for stimulation vs. baseline. Each point represents a specific cell type/stimulation for which the TF and targets were significantly altered ($p<0.05$). Colours are summarised per general cell type. R and p values are shown for Pearson correlation. (E) Top uniquely enriched TF target sets (by magnitude of NES) per cell type/stimulation vs. baseline.

Fig 4. | Differential ligand-receptor interactions driven by stimulation conditions.

Upregulated ligand-receptor interactions were predicted per condition compared to baseline with MultiNicheNet. (A) Overall similarity of the intercellular networks per condition (defined by the top 2000 upregulated interactions) compared by Jaccard indices. Three groups of similar conditions by signalling (BCS and LPS; IL-2, CytoStim™ and anti-CD3; TGF-β1, TNF-α and IL-1β) were defined and in (B) the top 20 upregulated interactions are shown for each group. (C) Summary of the top 50 upregulated interactions for the IFN-α and TGF-β1 conditions. (D) Highlighted supporting data for key ligand-receptor interactions in the IFN-α and TGF-β1 conditions. Data shown per ligand-receptor and sender-receiver cell (1 per row), from left to right are: scaled ligand-receptor pseudo-bulk expression product and sender/receiver cell presence per donor/condition; fraction of cells expressing ligand/receptor; downstream ligand activity (up- or down-regulated target genes) in receiver cells. (E) Expression of key ligands and receptors in specific cell types and stimulation conditions. Data are summarised with each point representing mean value per cell type/donor/stim. (E) Enriched Reactome pathways in each cell type, for IFN-α and TGF-β1 conditions compared to baseline. Enrichment derived from over-representation of genes that were up- or down-regulated ($p<0.05$), with colour representing direction multiplied by the significance (inverse log10 p-value). The top 40 pathways by mean absolute deviation of plotted values across all cell types and conditions are shown.

Fig. 5 | Cell type-specific signatures of disease within immunomodulatory conditions. (A) Gene set enrichment of cell type-specific disease gene sets (defined as $p<0.01$, log2-fold change >0.5; disease vs. healthy) from bulk sorted PBMCs (ImmunexUT dataset - rheumatoid arthritis, RA; systemic lupus erythematosus, SLE; systemic sclerosis, SSc) within ranked gene profiles (ranked by Wald stat; logFC/lfcSE; stimulation vs. baseline) of matching cell types of stimulated PBMC profiles. Enrichment is summarised as normalised enrichment score (NES) and overlap of differentially expressed genes (DEGs) between disease and stimulation (defined as $p<0.01$, log2-fold change >0.5; stimulated vs. baseline) by Jaccard index. (B) UMAP dimensional reduction of SLE and normal single PBMCs with mapped cell

type labels. Overall proportions for cell types with n>=100 are shown. (C) Jaccard indices of per-cell type upregulated DEGs ($p<0.05$) from SLE vs. normal cells, compared to upregulated DEGs from each cell type/stimulation vs. baseline. (D) Summary of the top 50 upregulated interactions in SLE vs. normal. (E) Jaccard indices of the top 2000 upregulated interactions from SLE compared to those from each stimulation condition. (F) Shared and unique upregulated interactions within the top 2000 for SLE vs. normal, and IFN-α vs baseline. The top 15 interactions from unique SLE, shared and unique IFN-α are shown. Up to 3 interactions are shown per cell type pair.

Supplementary figure legends

Supplementary Fig. 1

(A) UMAP dimensional reductions of cells by cell type, donor, stimulation condition and batch (pre- and post-integration). (B) Expression of cell type marker genes per final annotation (scaled per gene). (C) Total number of cells captured for each cell type. (D) Proportion of cell types per donor across each stimulation. (E) Proportion of cell types per donor summarised as box plots across each stimulation with Propeller compositional assessment for each condition vs. baseline. (F) Donor-level summary of cell cycle phase per cell type/stimulation condition with Wilcoxon test for each condition vs. baseline. * $p<0.05$; ** $p<0.01$; *** $p<0.001$; **** $p<0.001$.

Supplementary Fig. 2

(A) Log2-fold changes for top 4 differentially expressed genes (DEGs) per lineage (B, T, ILC, myeloid) by lowest p-values, for each stimulation vs. baseline. (B) Heatmap of all log2-fold changes vs. baseline for a set of 4,000 most variable genes across pseudo-bulk transcriptomic profiles. Each column represents a minor cell type/stim, annotated per general cell type. Rows (genes) were clustered with K-means clusters ($k = 7$) with curated enriched pathways shown for each cluster (GO BP and Reactome annotations).

Supplementary Fig. 3

Upregulated ligand-receptor interactions were predicted per condition compared to baseline with MultiNicheNet. (A) Pairwise comparisons by Jaccard index of networks generated by taking the top N ligand-receptor interactions (network edges) by prioritisation score. The threshold of top 2000 edges was selected to give maximal distinction between conditions and is highlighted on the plots. (B) Up to 5 top unique ligand-receptor network edges are shown per condition. (C) Top 50 interactions per condition vs. baseline. Arrows indicate direction of signalling from sender to receiver cell type. (D) and (E) highlight the supporting data for the

top 50 upregulated ligand-receptor interactions in the IFN-α and TGF-β1 conditions, respectively, compared to baseline. Data shown per ligand-receptor and sender-receiver cell (1 per row), from left to right are: scaled ligand-receptor pseudo-bulk expression product and sender/receiver cell presence per donor/condition; downstream ligand activity (up- or down-regulated target genes) in receiver cells; cell type-specificity and fraction of cells expressing ligand/receptor; summary of evidence for interaction (Omnipath).

Supplementary Fig. 4

(A) Gene set enrichment of cell type-specific disease gene sets (defined as $p<0.01$, log2-fold change >0.5; disease vs. healthy) from bulk sorted PBMCs (ImmunexUT dataset -systemic lupus erythematosus (SLE), idiopathic inflammatory myopathy (IIM), systemic sclerosis (SSc), mixed connective tissue disease (MCTD), Sjögren's syndrome (SjS), rheumatoid arthritis (RA), Behçet's disease (BD), adult-onset Still's disease (AOSD), ANCA-associated vasculitis (AAV), or Takayasu arteritis (TAK)) within ranked gene profiles (ranked by Wald stat; logFC/lfcSE; stimulation vs. baseline) of matching cell types of stimulated PBMC profiles. Enrichment is summarised as normalised enrichment score (NES; shown by colour). Overlap of significant gene sets between disease and stimulation (defined as $p<0.01$, log2-fold change >0.5; stimulated vs. baseline) was also assessed by Jaccard index (shown by size). (B) Reannotation of SLE and normal cells from a single-cell RNA-seq dataset to match cell type labels. (C) UMAP dimensional reduction showing the clustering of SLE and normal cells. (D) Number of upregulated differentially expressed genes (DEGs) per cell type in pseudo bulk profiles of SLE cells vs. healthy control. (E) Comparison of transcriptomic profiles from *in vivo* mouse cytokine treatment [5] vs. *in vitro* human PBMC stimulations, for equivalent cell type annotations and conditions used in both datasets. Size indicates Jaccard index of DEGs per cell type/condition, defined as those with $p<0.05$. Colour indicates Spearman correlation of log2-fold changes for all genes with direct or orthologous identifiers between human and mouse. (F) Summary of the number of DEGs per cell type/condition from *in vivo* mouse cytokine treatment.

Supplementary Fig. 5

(A) Gene set enrichment of cell type-specific disease gene sets (defined as $p<0.01$, log2-fold change >0.5; disease vs. healthy) from bulk sorted PBMCs (ImmunexUT dataset -systemic lupus erythematosus (SLE), idiopathic inflammatory myopathy (IIM), systemic sclerosis (SSc), mixed connective tissue disease (MCTD), Sjögren's syndrome (SjS), rheumatoid arthritis (RA), Behçet's disease (BD), adult-onset Still's disease (AOSD), ANCA-associated vasculitis (AAV), or Takayasu arteritis (TAK)) within ranked gene profiles (ranked by Wald stat; logFC/lfcSE; stimulation vs. baseline) of matching cell types of stimulated PBMC profiles. Enrichment is summarised as normalised enrichment score (NES; shown by colour). Overlap of significant gene sets between disease and stimulation (defined as $p<0.01$, log2-fold change >0.5; stimulated vs. baseline) was also assessed by Jaccard index (shown by size). (B) Reannotation of SLE and normal cells from a single-cell RNA-seq dataset to match cell type labels. (C) UMAP dimensional reduction showing the clustering of SLE and normal cells. (D) Number of upregulated differentially expressed genes (DEGs) per cell type in pseudo bulk profiles of SLE cells vs. healthy control. (E) Comparison of transcriptomic profiles from *in vivo* mouse cytokine treatment [5] vs. *in vitro* human PBMC stimulations, for equivalent cell type annotations and conditions used in both datasets. Size indicates Jaccard index of DEGs per cell type/condition, defined as those with $p<0.05$. Colour indicates Spearman correlation of log2-fold changes for all genes with direct or orthologous identifiers between human and mouse. (F) Summary of the number of DEGs per cell type/condition from *in vivo* mouse cytokine treatment.

Figure 1

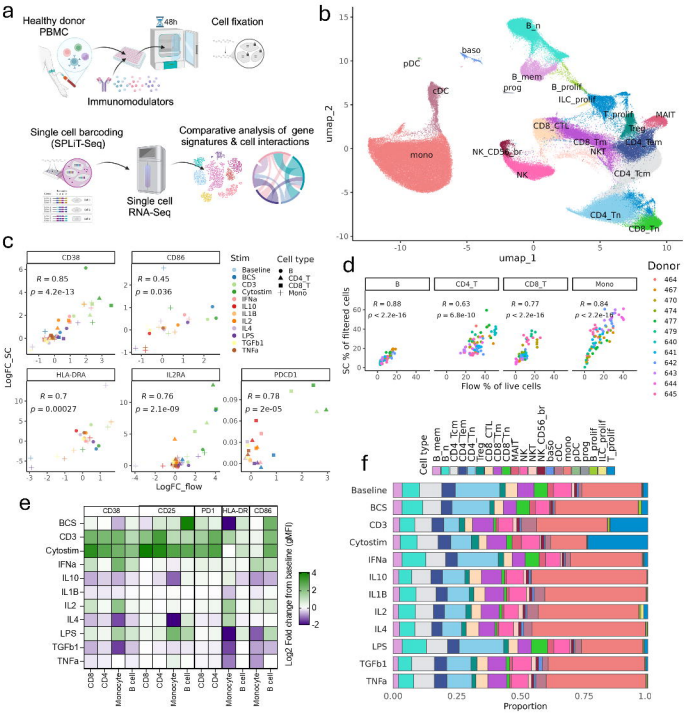
a
Healthy donor PBMC
48h
Cell fixation
Immunomodulators
Single cell barcoding (SPLiT-Seq)
Single cell RNA-Seq
Comparative analysis of gene signatures & cell interactions
b
umap_1
umap_2
B_n
baso
pDC
B_mem
prog
cDC
B_prolif
ILC_prolif
MAIT
T_prolif
CD8_CTL
Treg
mono
NK_CD56_br
CD8_Tm
CD4_Tem
NKT
NK
CD4_Tcm
CD4_Tn
CD8_Tn
c
CD38
CD86
HLA-DRA
IL2RA
PDCD1
R = 0.85
ρ = 4.2e-13
R = 0.45
ρ = 0.036
R = 0.7
ρ = 0.00027
R = 0.76
ρ = 2.1e-09
R = 0.78
ρ = 2e-05
LogFC_SC
LogFC_flow
Stim
Baseline
BCS
CD3
Cytostim
IFNa
IL10
IL1B
IL2
IL4
LPS
TGFb1
TNFa
Cell type
B
CD4_T
CD8_T
Mono
d
B
CD4_T
CD8_T
Mono
R = 0.88
ρ < 2.2e-16
R = 0.63
ρ = 6.8e-10
R = 0.77
ρ < 2.2e-16
R = 0.84
ρ < 2.2e-16
SC % of filtered cells
Flow % of live cells
Donor
464
467
470
474
477
479
640
641
642
643
644
645
e
CD38
CD25
PD1
HLA-DR
CD86
BCS
CD3
Cytostim
IFNa
IL10
IL1B
IL2
IL4
LPS
TGFb1
TNFa
CD8+
CD4+
Monocyte-
B cell+
Log2 Fold change from baseline (gMFI)
f
Cell type
B_mem
CD4_Tcm
CD4_Tem
CD4_Tn
Treg
CD8_CTL
CD8_Tem
CD8_Tn
MAIT
NK
NKT
NK_CD56_br
baso
cDC
prog
pDC
B_prolif
ILC_prolif
T_prolif
Baseline
BCS
CD3
Cytostim
IFNa
IL10
IL1B
IL2
IL4
LPS
TGFb1
TNFa
0.00
0.25
0.50
0.75
1.0
Proportion

Figure 2

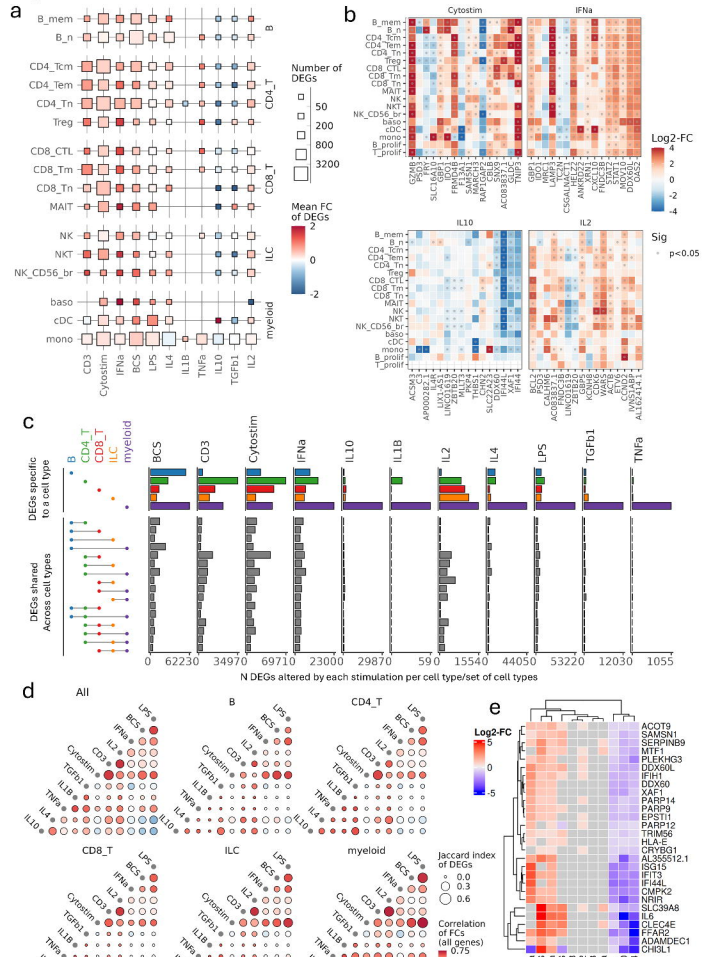
a
B_mem
B_n
B
CD4_Tcm
CD4_Tem
CD4_Tn
Treg
CD4_T
CD8_CTL
CD8_Tm
CD8_Tn
MAIT
CD8_T
NK
NKT
NK_CD56_br
ILC
baso
cDC
mono
myeloid
CD3
Cytostim
IFNa
BCS
LPS
IL4
IL1B
TNFa
IL10
TGFb1
IL2
Number of DEGs
50
200
800
3200
Mean FC of DEGs
2
0
-2
b
Cytostim
IFNa
IL10
IL2
Log2-FC
4
2
0
-4
Sig
p<0.05
c
DEGs specific to a cell type
DEGs shared Across cell types
BCS
CD3
Cytostim
IFNa
IL10
IL1B
IL2
IL4
LPS
TGFb1
TNFa
0
62230
34970
69710
23000
29870
590
15540
44050
53220
12030
1055
N DEGs altered by each stimulation per cell type/set of cell types
d
All
B
CD4_T
CD8_T
ILC
myeloid
Jaccard index of DEGs
0.0
0.3
0.6
Correlation of FCs (all genes)
0.75
0.00
-0.75
e
Log2-FC
5
0
-5
ACOT9
SAMSN1
SERPINB9
MTF1
PLEKHG3
DDX60L
IFIH1
DDX60
XAF1
PARP14
PARP9
EPSTI1
PARP12
TRIM56
HLA-E
CRYBG1
AL355512.1
ISG15
IFIT3
IFI44L
CMPK2
NRIR
SLC39A8
IL6
CLEC4E
FFAR2
ADAMDEC1
CHI3L1

Figure 3

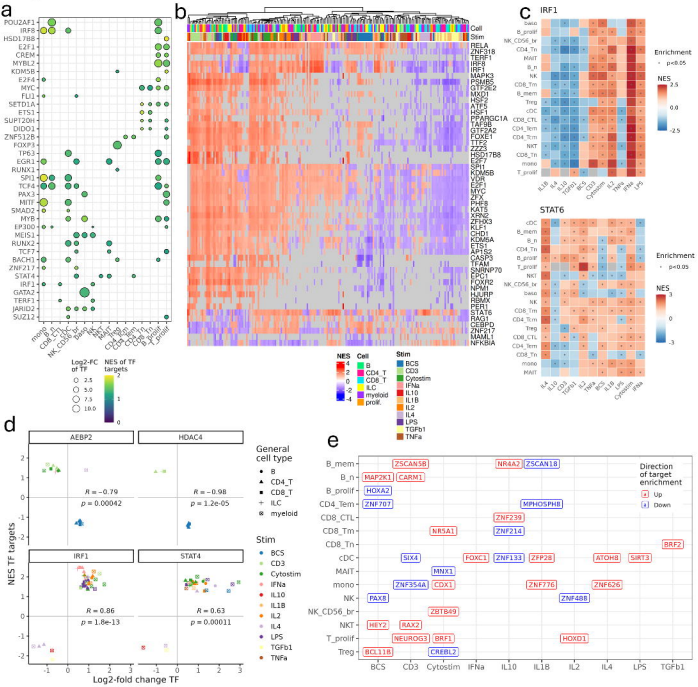
a
b
c
IRF1
STAT6
Enrichment
p<0.05
NES
Log2-FC of TF
NES of TF targets
Cell
Stim
d
AEBP2
HDAC4
IRF1
STAT4
R = −0.79
p = 0.00042
R = −0.98
p = 1.2e-05
R = 0.86
p = 1.8e-13
R = 0.63
p = 0.00011
NES TF targets
Log2-fold change TF
General cell type
B
CD4_T
CD8_T
ILC
myeloid
Stim
BCS
CD3
Cytostim
IFNa
IL10
IL1B
IL2
IL4
LPS
TGFb1
TNFa
e
Direction of target enrichment
Up
Down
B_mem
B_n
B_prolif
CD4_Tem
CD8_CTL
CD8_Tm
cDC
MAIT
mono
NK
NK_CD56_br
NKT
T_prolif
Treg
ZSCAN18
NR4A2
MAP2K1
CARM1
HOXA2
ZNF707
MPHOSPHB
ZNF239
NR5A1
ZNF214
BRF2
SIX4
FOXC1
ZNF133
ZFP28
ATOH8
SIRT3
MNX1
ZNF354A
CDX1
ZNF776
ZNF626
PAX8
ZNF488
ZBTB49
HEY2
RAX2
NEUROG3
BRF1
HOXD1
BCL11B
CREB1L2
BCS
CD3
Cytostim
IFNa
IL10
IL1B
IL2
IL4
LPS
TGFb1

Figure 4

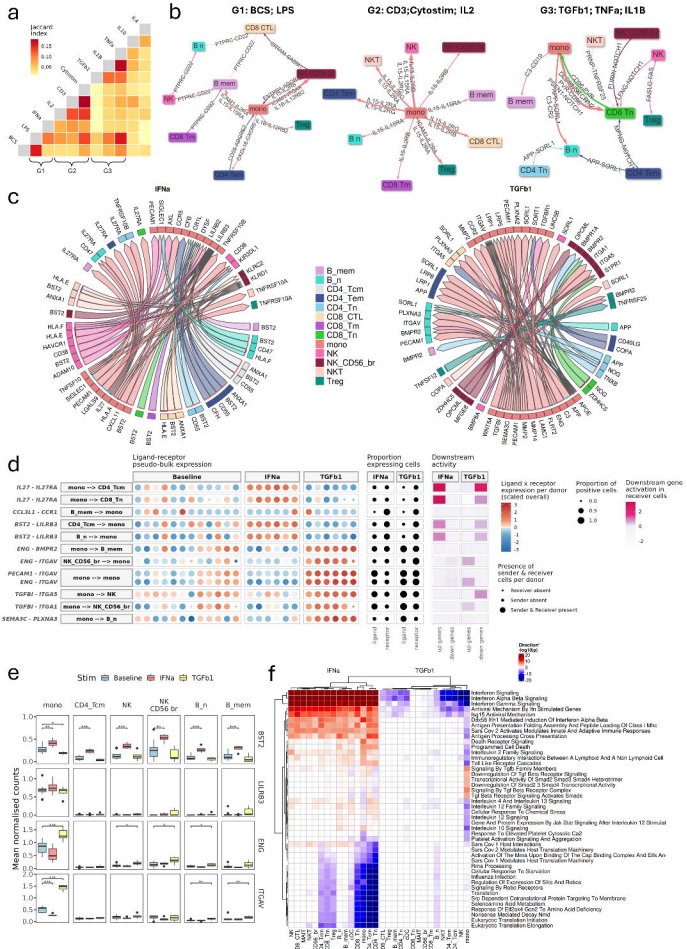
a
Jaccard Index
b
G1: BCS; LPS
G2: CD3;Cytostim; IL2
G3: TGFb1; TNFa; IL1B
c
IFNa
TGFb1
B_mem
B_n
CD4_Tcm
CD4_Tem
CD4_Tn
CD8_CTL
CD8_Tm
CD8_Tn
mono
NK
NK_CD56_br
NKT
Treg
d
Ligand-receptor pseudo-bulk expression
Baseline
IFNa
TGFb1
IL27 - IL27RA
mono --> CD4_Tcm
IL27 - IL27RA
mono --> CD8_Tn
CCL3L1 - CCR1
B_mem --> mono
B3T2 - LILRB3
CD4_Tcm --> mono
B3T2 - LILRB3
B_n --> mono
ENG - BMPR2
mono --> B_mem
ENG - ITGAV
NK_CD56_br --> mono
PECAM1 - ITGAV
mono --> mono
ENG - ITGAV
mono --> NK
TGFB1 - ITGA5
mono --> NK_CD56_br
SEMA3C - PLXNA3
mono --> B_n
Proportion expressing cells
Downstream activity
Ligand expression
Receptor expression
up genes
down genes
Ligand x receptor expression per donor (scaled overall)
Proportion of positive cells
Downstream gene activation in receiver cells
Presence of sender & receiver cells per donor
Receiver absent
Sender absent
Sender & Receiver present
Direction regulon
e
Stim
Baseline
IFNa
TGFb1
mono
CD4_Tcm
NK
NK CD56 br
B_n
B_mem
B3T2
LILRB3
ENG
ITGAV
Mean normalised counts
f
IFNa
TGFb1
Interferon Signaling
Interferon Alpha Beta Signaling
Interferon Gamma Signaling
Regulation Of Apoptosis Induced By Extracellular Signals
Sig Tf Actived Mechanism
Cd3/Cd28 Pin1 Mediated Induction Of Interferon Alpha Beta
Antigen Presentation Folding Assembly And Peptide Loading Of Class I Mhc
Sars Cov 2 Activates Modulates Innate And Adaptive Immune Responses
Class I Mhc Mediated Antigen Presentation
Death Receptor Signalling
Programmed Cell Death
Interleukin 3 Family Signaling
Immunoregulatory Interactions Between A Lymphoid And A Non Lymphoid Cell
Tnf Receptor Superfamily
Signaling By Tgfb Family Members
Downregulation Of Tgf Beta Receptor Signaling
Transcriptional Activity Of Smad2 Smad3 Smad4 Heterotrimer
Regulation Of Tgf Beta Receptor Signaling Activity
Signaling By Tgf Beta Receptor Complex
Tgf Beta Receptor Signaling Activates Smads
Interleukin 4 And Interleukin 13 Signaling
Cellular Response To Hypoxia
Cellular Response To Chemical Stress
Interleukin 12 Signaling
Gene And Protein Expression By Jak Stat Signaling After Interleukin 12 Stimulation
Interleukin 10 Signaling
Cellular Response To Extracellular Matrix
Platelet Activation Signaling And Aggregation
Sars Cov 1 Host Interactions
Sars Cov 2 Modulates Host Translation Machinery
Activation Of The Mrna Upon Binding Of The Cap Binding Complex And Eifs And Subsequent Assembly Of 43s Host Translation Machinery
Rna Processing
Cellular Response To Stimulation
Signaling By Notch
Regulation Of Expression Of Slits And Robos
Signaling By Robo Receptors
Translation
Srp Dependent Cotranslational Protein Targeting To Membrane
Cellular Response To Hypoxia
Response Of Eif2ak4 Gcn2 To Amino Acid Deficiency
Nonsense Mediated Decay Nmd
Eukaryotic Translation Initiation
Eukaryotic Translation Elongation
Direction regulon
up
0
down
mono
NK
CD8_CTL
CD8_Tn
CD4_Tcm
NK_CD56_br
B_n
B_mem
CD8_Tm
CD4_Tem
CD4_Tn

Figure 5

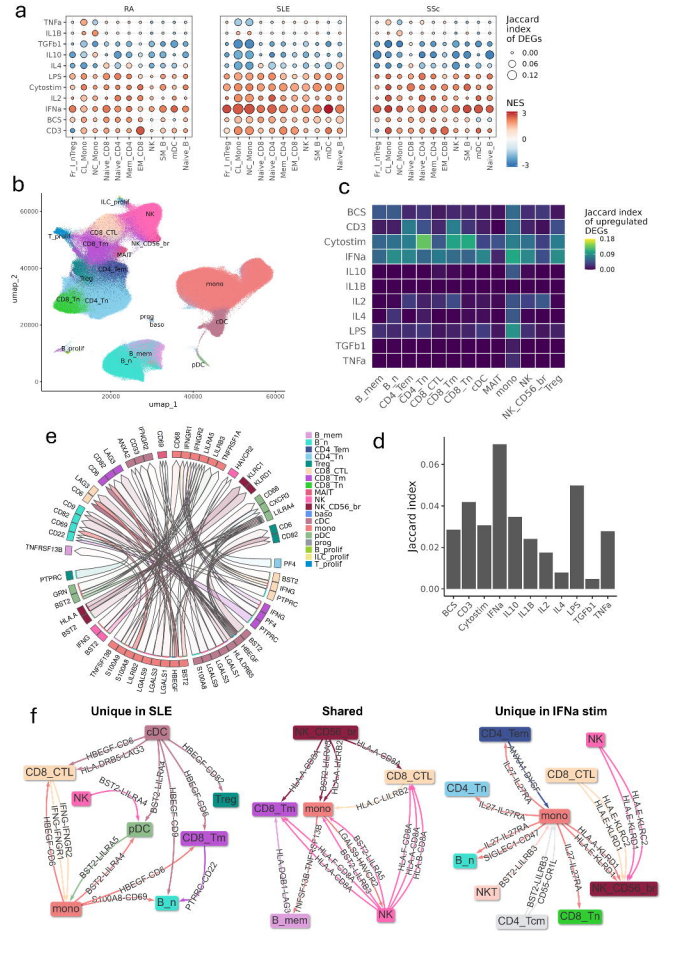

a
RA
SLE
SSc
TNFa
IL1B
TGFb1
IL10
IL4
LPS
Cytostim
IL2
IFNa
BCS
CD3
Fr_I_nTreg
CL_Mono
NC_Mono
Naive_CD8
Naive_CD4
Mem_CD4
EM_CD8
NK
SM_B
mDC
Naive_B
Jaccard index of DEGs
0.00
0.06
0.12
NES
3
0
-3
b
umap_1
umap_2
ILC_prolif
NK
T_prolif
CD8_CTL
CD8_Tm
NK_CD56_br
MAIT
CD4_Tem
Treg
CD8_Tn
CD4_Tn
mono
prog
baso
cDC
B_prolif
B_mem
B_n
pDC
c
BCS
CD3
Cytostim
IFNa
IL10
IL1B
IL2
IL4
LPS
TGFb1
TNFa
Jaccard index of upregulated DEGs
0.18
0.09
0.00
B_mem
B_n
CD4_Tem
CD4_Tn
Treg
CD8_CTL
CD8_Tm
CD8_Tn
MAIT
NK
NK_CD56_br
baso
cDC
mono
pDC
prog
B_prolif
ILC_prolif
T_prolif
e
d
Jaccard index
f
Unique in SLE
Shared
Unique in IFNa stim